Ammonia oxidation rate is a fundamental control on thaumarchaeal lipid composition and the TEX_{86} proxy

Sarah J. Hurley[1*§], Felix J. Elling[2§], Martin Könneke[2], Carolyn Buchwald[3], Scott D. Wankel[3], Alyson E. Santoro[4], Julius S. Lipp[2], Kai-Uwe Hinrichs[2], Ann Pearson[1*]

1. Department of Earth and Planetary Sciences, Harvard University, Cambridge, Massachusetts 02138, USA 2. Organic Geochemistry Group, MARUM - Center for Marine Environmental Sciences & Department of Geosciences, University of Bremen, Bremen, 28359, Germany 3. Department of Marine Chemistry and Geochemistry, Woods Hole Oceanographic Institution, Woods Hole, Massachusetts 02543, USA 4. Horn Point Horn Point Laboratory, University of Maryland Center for Environmental Science, Cambridge, Maryland 21613, USA

Submitted to Proceedings of the National Academy of Sciences of the United States of America

Archaeal membrane lipids known as GDGTs are the basis of the TEX_{86} sea surface temperature (SST) proxy. Because GDGTs are thought to be produced mainly by planktonic Thaumarchaeota – the ocean's major aerobic oxidizers of ammonia – the mechanistic underpinning of the TEX_{86}-SST proxy remains a mystery: How do TEX_{86} values predict SSTs, when the maximum activity of Thaumarchaeota occurs below the surface mixed layer? Here we investigated the TEX_{86} proxy using isothermal studies of the model thaumarchaeon *Nitrosopumilus maritimus* SCM1. By employing continuous-culture methods we avoided the potential confounding variables that can be associated with experiments in batch cultures. The results show that TEX_{86} and the ring index (RI) scale inversely (R^2 = 0.65 and 0.77, respectively) with the ammonia oxidation rate, indicating that TEX_{86} and RI depend on available reducing power. The TEX_{86} ratio decreases by 5.4°C of SST-calibrated temperature over a 5.5 fmol cell^{-1} day^{-1}decrease in ammonia oxidation rate. This finding reconciles other recent experiments that have identified growth stage and oxygen availability as variables affecting TEX_{86}. Depth-dependent TEX_{86} profiles from the marine water column produce similar patterns of minimum TEX_{86} values at the depth of maximum ammonia oxidation rates, consistent with the chemostat results. Our findings suggest that the integrated signal of GDGTs reaching the sediments is a function of the dynamics of ammonia oxidation in the overlying water column. The TEX_{86}-SST relationship likely is governed by the structure of the nutricline, rather than directly controlled by temperature.

TEX86 | Thaumarchaeota | GDGT | Continuous Culture

Introduction

The TEX_{86} sea surface temperature (SST) proxy is a paleothermometer based on the glycerol dibiphytanyl glycerol tetraether (GDGT) membrane lipids of marine Archaea (1). GDGTs accumulate in sediments and are preserved in the geologic record on the order of 100 million years, spanning temporally and geographically diverse events in Earth history (*e.g.,* (2–4) and often agreeing well with other proxy records (*e.g.,* (5, 6).

The major source of GDGTs to ocean sediments is assumed to be ammonia-oxidizing archaea (AOA) affiliated with the phylum Thaumarchaeota (formerly Marine Group I Crenarchaeota (7, 8). Thaumarchaeota produce intact polar GDGTs (IPL-GDGTs) with glycosidic headgroups (9, 10) attached to isoprenoid core lipids — hydrocarbon backbones linked at each end via ether bonds to glycerol moieties (11–13). Similar lipids may also be produced by marine planktonic Euryarchaeota (14) and sedimentary Archaea (15, 16). GDGT core lipids contain from zero to four cyclopentane rings (GDGT-0 to GDGT-4) and sometimes include an additional cyclohexane ring (*e.g.*, in crenarchaeol) (Fig. S1). The TEX_{86} ratio defines a relationship between a specific subset of these GDGTs (Eq. S3; (1); this value is then calibrated empirically using surface sediments to annual mean SST (Eq. S4; (17, 18).

The physiological basis of cytoplasmic membrane adjustment in mesophilic Archaea, however, remains poorly understood. Because Thaumarchaeota perform the first step of nitrification (19), namely the oxidation of ammonia (NH_3) to nitrite (NO_2^-), their distribution correlates broadly with the nutricline, placing their primary habitat within and below the subsurface chlorophyll maximum, *i.e.*, well below the surface mixed layer and its SST (20–23). Additional evidence, including the ratio of GDGT-2 to GDGT-3 (24) and the ^{14}C content (25–27), confirms that the provenance of exported GDGTs is primarily sub-photic.

A causal relationship between water temperature and the TEX_{86} ratio thus appears incompatible with our current understanding of AOA physiology and ecology. TEX_{86} values of suspended material from sub-photic waters do not reflect *in situ* temperatures either in trend or magnitude (26, 28–33). Indeed, TEX_{86}-derived temperatures often reach their maximum values below 200 m depth, indicating that physiological effects other than temperature are important in determining environmental TEX_{86} signals.

A clue to explaining these observations comes from batch cultures of marine Thaumarchaeota. TEX_{86} values increase in later growth phases (34) and at lower O_2 concentrations (35). The commonality between these experiments is that both experienced a variable rate of energy supply. Because energy limitation has been suggested to be a defining feature of the Archaea (36), and GDGTs effectively reduce proton permeability and hence promote energy conservation (37, 38), we hypothesized that avail-

Significance

The membrane lipids of marine archaea form the basis of the sea surface temperature (SST) proxy called TEX_{86}. TEX_{86} has been used for paleoclimate reconstructions from the Jurassic to the present, although there remains no satisfactory explanation for how planktonic archaea are able to record SST, a question that is complicated by their low abundance in surface waters. Instead they are thought to be predominantly aerobic ammonia oxidizers, living mostly below the photic zone. Here we show that the TEX_{86} lipid ratio is a function of the metabolic energy flux, which is controlled by the nitrification rate. This implies that the TEX_{86} proxy is controlled by the nutrient structure of the water column, rather than directly by temperature.

Reserved for Publication Footnotes

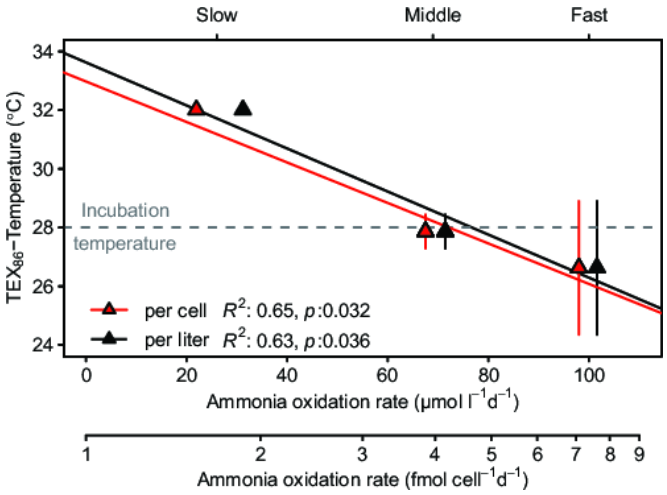

Fig. 1. TEX_{86}-derived temperatures of total GDGTs obtained from hydrolyzed *N. maritimus* biomass decrease a function of ammonia oxidation rates; cultures were maintained at steady state at 28 °C. Error bars represent multiple biomass harvests (n = 1 to 3) during the chemostat states.

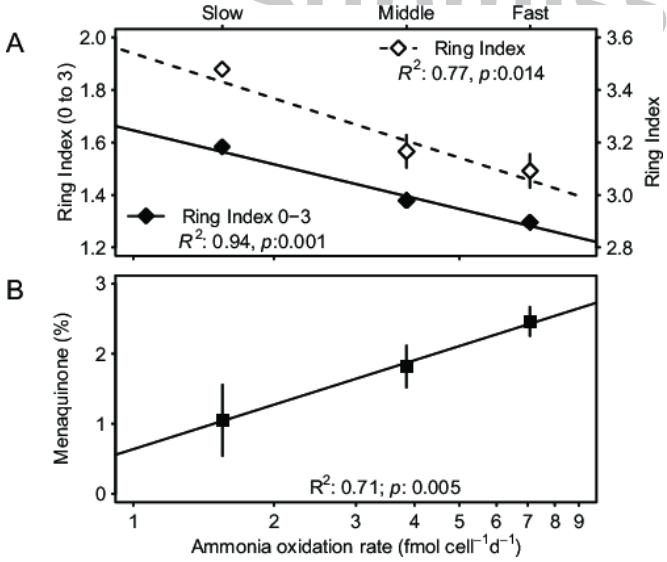

Fig. 2. Lipid ratios vary as a function of ammonia oxidation rate in an isothermal continuous culture of *N. maritimus*. The ring index of total GDGTs (white diamonds) and GDGTs -0, -1, -2, and -3 only (black diamonds) decrease at higher ammonia oxidation rate (A), corresponding to an increase in respiratory quinone (MK) abundance relative to total lipids (B). Error bars represent multiple biomass harvests (n = 1 to 3) during the chemostat states.

ability of adequate reducing equivalents, generated *via* an energy-dependent reverse electron flow from ammonia, could have a direct effect on GDGT distributions.

Here we performed a continuous culture (chemostat) experiment to isolate the influence of energy and e^--donor supply on the lipid composition of the marine AOA *N. maritimus* SCM1. Chemostat approaches have been valuable in characterizing the response of marine taxa to changing CO_2 concentrations (39, 40), and to nutrient limitation (41), each with the objective of isolating a component of physiological response. In our experiments with *N. maritimus*, the chemostat not only controls the growth and corresponding ammonia oxidation rate, but also maintains chemical and thermal stability of the growth conditions. This approach is fundamentally different from all previous batch culture (34, 35, 42) and mesocosm (43) studies of GDGT-producing planktonic

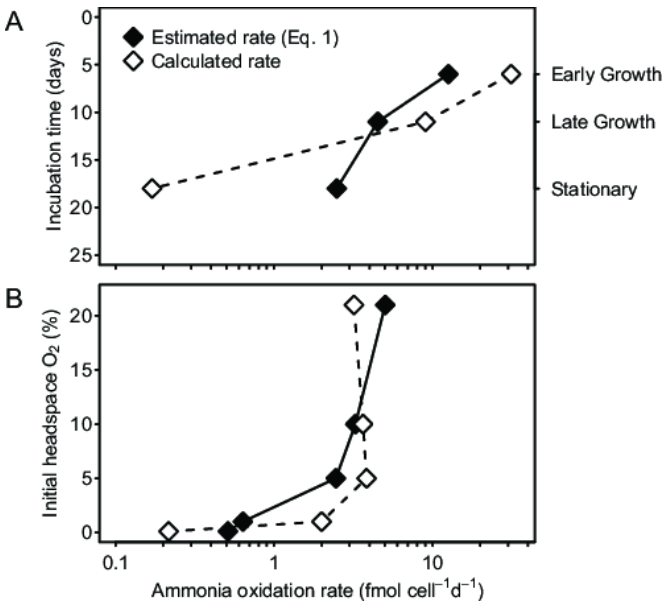

Fig. 3. Ammonia oxidation rates of previously published batch culture experiments (34, 35) were estimated from measured TEX_{86} values using the experimentally determined relationship of Eq. 1 (black diamonds) and calculated using reported cell densities and time-dependent concentration of NO_2^- (white diamonds). Batch cultures from (34) yield higher TEX_{86} values and lower ammonia oxidation rates in later growth phases as the ammonia supply is depleted (from early growth phase to stationary phase; A). Batch cultures from (35) under oxygen limitation similarly yield higher TEX_{86} values and lower ammonia oxidation rates as O_2 decreases (B).

archaea, in which several potentially competing variables such as growth rate, temperature, chemical composition of the medium, and community assemblage simultaneously influenced the lipid distributions.

Results

Lipid response to controlled energy supply. We cultivated an isothermal (28°C) continuous culture of *N. maritimus* (Fig. S2) to steady-state at each of three dilution rates, corresponding to doubling times (T_d) of 71 h (slow state), 30 h (middle state), and 22 h (fast state); thereby maintaining the system in continuous culture for 6 months over the course of the experiments. Nearly identical cell concentrations (1.4-1.9 10^7 cells ml^{-1}, Fig. S3, Table S1) were achieved at the different growth rates by limited provision of ammonia (inflow *ca.* 150 µM). Ammonia oxidation rates, as measured by the production of NO_2^-, were 31.2, 71.4, and 101.6 µmol l^{-1} d^{-1} (1.6, 3.9, and 7.1 fmol $cell^{-1}$ d^{-1}), respectively. The concentration of NO_2^- in the chemostat varied by a maximum of 7% across all stages (mean value 132.5 µM), and the pH remained within 0.07 units of the mean value (7.64). Biomass harvested during each state was directly hydrolyzed to remove polar head groups and obtain total GDGTs, while non-hydrolyzed biomass was extracted to measure respiratory quinones and IPL-GDGTs (for structures see Fig. S1).

The TEX_{86}-derived temperatures calculated from total GDGTs were lower at higher ammonia oxidation rates (*i.e.*, shorter doubling times). TEX_{86}-temperatures ranged from 32.0°C during the slow-growth state to 26.6°C during the fast-growth state, representing up to 4°C deviation from the actual growth temperature of 28°C (Fig. 1a). The relationship between TEX_{86}-derived temperature and cell-specific ammonia oxidation rate (Φ) was linear:

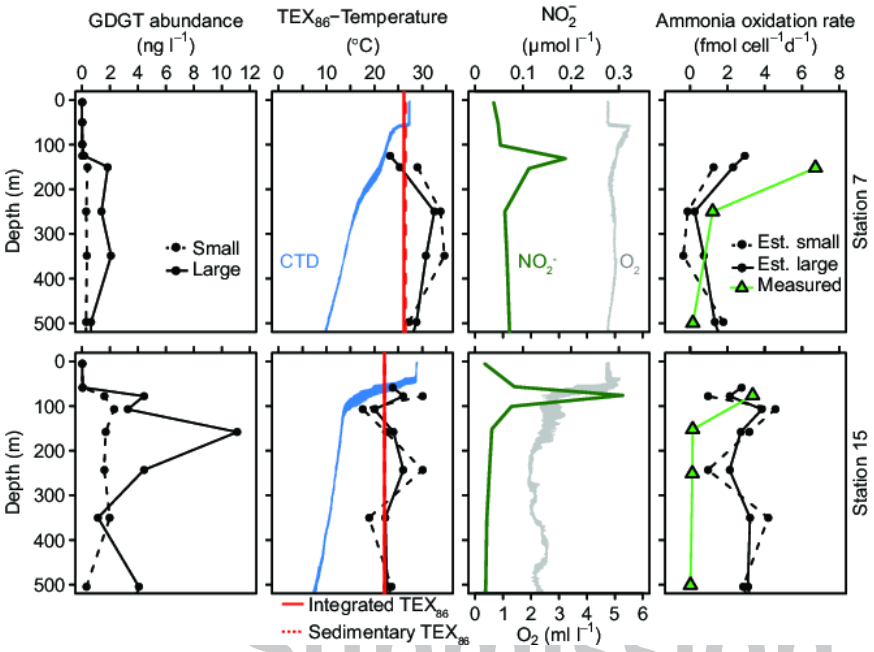

Fig. 4. South Atlantic Ocean water column properties support the relationship between TEX_{86} and ammonia oxidation rate (22.5°S 33.0°W: Station 7, 2.7°S 28.5°W: Station 15). Column 1: GDGT abundance in small (0.3-0.7 µm) and large (0.7-53 µm) suspended particulate size classes. Column 2: TEX_{86} values from small and large size classes do not reflect *in situ* measured temperatures. Water-column integrated and nearest sedimentary TEX_{86} values agree, reflecting the export signal of GDGTs from sub-surface waters. Column 3: Nitrite and oxygen profiles. Column 4: Ammonia oxidation rates estimated from TEX_{86} values of GDGTs (using Eq. 1) qualitatively agree with measured rates converted to cell-specific values *via* GDGT abundance.

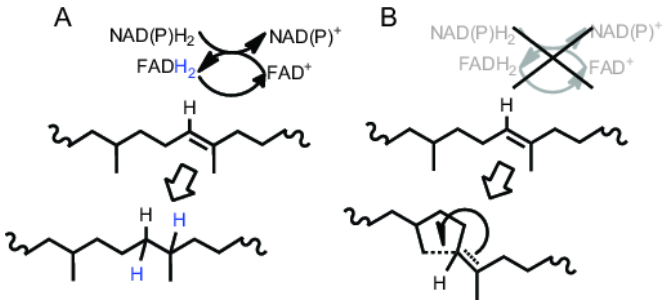

Fig. 5. Proposed synthesis of GDGT-0 from two molecules of DGGGP includes a saturation step (A) mediated by GGR and requiring the cofactors $FADH_2$ and NAD(P)H_2. Electron limitation (B) may slow the regeneration of one or more of these cofactors, causing internal cyclization rather than saturation.

$$T_{TEX86} = -3.46 \times 10^{-2}\,\Phi + 32.98\ (R^2 = 0.65,\ p\text{-}value = 0.032,\ n = 6) \quad [1]$$

The trend in TEX_{86}-derived temperatures reflects an underlying change in the cyclization of total GDGTs. The most abundant compounds (crenarchaeol and GDGT-2) increased with lower Φ at the expense of GDGT-0 and GDGT-1 (Table S2). GDGTs of minor abundance (GDGT-3 and the crenarchaeol regioisomer) did not show a systematic variation with Φ. Accordingly, the GDGT ring index (RI; Eq. S5), a cyclization metric, increased with lower Φ (R^2 = 0.77, *p-value* = 0.014, n = 6; Fig. 2a; Eq. S7), and the RI calculated only from GDGTs with zero to three cyclopentane rings (GDGT-0 to GDGT-3; Eq. S6) had the best linear fit with Φ (R^2 = 0.94, *p-value* = 0.001, n = 6; Fig. 2a; Eq. S8).

The relative abundance of respiratory menaquinones (MK) – isoprenoid lipids that act as intra-membrane electron and proton carriers within the respiratory chain (*e.g.*, (44)– decreased at lower Φ, representing from 2.5 to 1.0% of total lipids (Fig. 2b). This is consistent with a down-regulated electron transport chain in more slowly-metabolizing cells. The relationship between MK abundance and Φ was a linear function with a goodness of fit similar to the RI relationships (Eq. S9, R^2 = 0.71, *p-value* = 0.005, n = 8; Fig. 2b).

Implications for previous batch culture experiments. Batch cultures grown at different metabolic energy levels provide the closest experimental analogs to our chemostat results. Harvesting batch cultures during successive growth phases (*i.e.,* early growth, late growth, and stationary phase) presumably samples decreasing ammonia oxidation rates in an system that is becoming more energy-limited as the ammonia supply is used up (34). Varying the O_2 concentration should similarly control the ammonia oxidation rate by limiting the availability of e^--acceptor, instead of (or co-limiting with) the e^--donor (35). To examine this effect, we used the TEX_{86}-ammonia oxidation rate regression (Eq. 1) to estimate the cell-specific ammonia oxidation rates for *N. maritimus* in these two batch culture systems (Fig. 3). We then used the reported cell densities and time-dependent concentration of NO_2^- in the batch cultures to independently calculate the ammonia oxidation rates and compare them to the TEX_{86}-derived estimates.

Elling et al. (34) showed that the apparent temperature calculated from TEX_{86} values increases over the course of a batch culture. Using these TEX_{86} values in Eq. 1, the estimated cell-specific ammonia oxidation rates decrease by *ca.* 12 fmol cell^{-1} d^{-1} from early growth phase, when there is excess substrate, to stationary phase, when substrate is depleted (Fig. 3a). The NO_2^--calculated oxidation rates similarly decreased from early growth phase to stationary phase, however the magnitude of change is greater.

In batch cultures incubated with different headspace O_2 concentrations, the apparent TEX_{86}-temperatures increased at lower O_2 concentrations (35). The cell-specific ammonia oxidation rates estimated using these TEX_{86} values in Eq. 1 are therefore lower, decreasing by *ca.* 5 fmol cell^{-1} d^{-1} under oxygen-limiting conditions (Fig. 3b). These estimated rates agree well with the ammonia oxidation rates determined directly from the cell densities and NO_2^- concentrations.

In all three culture systems – chemostat, high-nutrient batch (34) , and O_2-limiting batch (35) – the trends in TEX_{86}-estimated ammonia oxidation rates are consistent with independently calculated NO_2^- production rates. These experiments with *N. maritimus* point to a common TEX_{86} response, in which TEX_{86}-

derived temperatures increase as ammonia oxidation rate decreases.

Applicability to marine water columns. To test the TEX_{86}-ammonia oxidation rate relationship in the environment, we measured TEX_{86} ratios and nitrification rates for the upper water column of the South Atlantic Ocean (Fig. 4). We calculated a mass-weighted integration of TEX_{86} values to approximate the export signal from the upper water column (see SI, Table S3) and compared it to the nearest sedimentary value from the global calibration dataset (17). At Station 2, the integrated TEX_{86}-temperature and the nearest sedimentary TEX_{86} value agree with measured SST within calibration error (Fig. 4, column 2. At Station 15, the integrated and sedimentary TEX_{86} values appear colder than measured SST, potentially due to productivity differences associated with equatorial upwelling (Fig. S5). At most individual depths, TEX_{86}-derived temperatures broadly agree between suspended particulate matter (SPM) from large (0.7-53 μm) and small (0.3-0.7 μm) particle size classes; however, TEX_{86} values reflect neither SSTs nor *in situ* growth temperatures (Fig. 4, column 2). The TEX_{86} profiles show minima at the depth of the primary NO_2^- concentration maxima around 100-150 m and then increase with depth through at least 250 m (Fig. 4, columns 2-3; SI). The estimated ammonia oxidation rates (calculated using the experimentally determined TEX_{86} relationship, Eq. 1) therefore also show maxima at the NO_2^- concentration maxima, and minima below this depth (Fig. 4, column 4). The estimated ammonia oxidation rates qualitatively mirror the nitrification rates measured using isotopic tracer approaches (Fig. 4, column 4), although different depth resolution between the two data sets prevents an exact comparison.

Cell-specific ammonia oxidation rates in the chemostat (1.6 to 7.1 fmol $cell^{-1}$ day^{-1}) – as well as those estimated for previous batch cultures (34, 35) and the marine water column – fall well within activities of natural assemblages in pelagic (0.2 -15 fmol $cell^{-1}$ day^{-1}; (23) and coastal settings (10 fmol $cell^{-1}$ day^{-1}; (45). The cell-specific rate during the slow chemostat stage additionally resembled the pelagic AOA enrichment, *Candidatus* Nitrosopelagicus brevis (2 fmol NO_2^- $cell^{-1}$ day^{-1}; T_d = 98 h; (46, 47), as well as North Sea enrichments (2-4 fmol NO_2^- $cell^{-1}$ day^{-1}; (48).

Discussion

The TEX_{86} and RI ratios describe the relative numbers of rings (cyclopentane or cyclohexane) within the biphytanyl moieties of GDGTs. Because thermophilic archaea employ cyclization as an adaptation to growth temperature (49–51), the TEX_{86} ratio in marine archaea was assumed to depend primarily on temperature (1). Although it is now acknowledged that other factors such as community dynamics and regional patterns may affect TEX_{86} calibrations (18, 52, 53), and that *in situ* temperature and TEX_{86} are decoupled in the global subsurface ocean (*e.g.*, (28, 31, 32), these arguments remain centered around a temperature-driven response.

However, sole or primary dependence of TEX_{86} on growth temperature seems unlikely given that additional environmental and physiological factors affect lipid composition in other Archaea (35, 54–56, 42). At the depth of maximum thaumarchaeal activity, between 100-500 m (*e.g.*, (20), most ocean waters have temperatures between 5-15°C (with the exception of polar latitudes). This is much colder and represents a smaller dynamic range than experiments performed with thermophiles, yet GDGTs of marine archaea consistently have higher RI values than thermophiles (34, 35, 54). GDGT monolayer membranes have been suggested to be an adaption that helps to minimize proton permeability, thus reducing maintenance energy and maximizing proton motive force (36–38). The high RI of marine mesophilic Thaumarchaeota suggests that energy conservation may be a greater influence on GDGT composition than temperature, pH, or other variables.

Metabolic adaptation of planktonic Archaea to energy limitation. The *in-situ* energetic stress imposed by low ammonia and/or O_2 availability – as well as the intrinsically low energetic yield of ammonia oxidation – may qualify the Thaumarchaeota as energetic extremophiles (36). This idea is consistent with studies that show a low half-saturation constant (K_m; NH_3 + NH_4^+) of 98-132 nM for ammonia oxidation by *N. maritimus* (57, 58), and it suggests adaptation to growth under conditions of constantly low energy flux, as typically found in open ocean waters. *N. maritimus* (as well as the recently characterized Thaumarchaeon *Candidatus* Nitrosopelagicus brevis) fixes inorganic carbon using an energy-efficient hydroxypropionate/hydroxybutyrate (HP/HB) pathway that minimizes input of chemical energy from ATP and yields the products acetate (HP/HB full cycle) and succinate (HP half cycle) (47, 59, 60).

Obligate or facultative mixotrophy in some Thaumarchaeota is also consistent with the idea that cells have optimized their ability to survive low e^--flux by accessing critical carbon substrates (60–62). The marine strains HCA1 and PS0 require low levels of 2-oxoglutarate, while the soil AOA *Nitrososphaera viennensis* needs pyruvate supplementation to grow. These organic compounds are precursors for synthesis of essential biomolecules, *e.g.*, amino acids, that are produced *via* an incomplete citric acid cycle. This suggests that these strains have partially suppressed the diversion of succinate through the HP half cycle. The co-assimilation of organic metabolites may be a strategy to conserve energy and reducing equivalents within the full HP/HB cycle by slowing the "shunt" through succinate to ensure sufficient e^- conservation for the production of acetyl-CoA.

The results of our chemostat growth experiments are consistent with this view of metabolic adaptation to energy stress. How, then, does this observation explain GDGT lipid ratios, in which RI and TEX_{86} values increase at greater ammonia limitation? In addition to promoting energy conservation through decreased proton permeability, we argue there may also be a biosynthetic explanation.

Cellular energy balance and the synthesis of GDGTs: The reducing power-limitation hypothesis. Most chemolithotrophs conserve only a small fraction of the energy obtained from the respiration of inorganic substrates, *i.e.*, most of the energy flux is dissimilatory. From the conserved fraction, they must generate adequate reducing power for biosynthetic processes, and in most cases – including AOA – this requires energy-dependent reverse electron transport. For example, the electrochemical potential of the NH_4^+/NO_2^- redox couple is insufficient to reduce $NAD(P)^+$ to $NAD(P)H_2$. However, the synthesis of GDGT-0 from two molecules of the intermediate *sn*-2,3-di-*O*-geranylgeranyl glycerol-1-phosphate (DGGGP) requires 14 H_2 equivalents in a reduction reaction mediated by the enzyme geranylgeranyl reductase (GGR; Fig. 5a,b; (63). A hypothetical gene coding for GGR is present in the genome of *N. maritimus* (64). The cofactor for GGR is $FADH_2$, and it is most likely regenerated by e^- supplied by $NAD(P)H_2$ (65). Thus, progression of the saturation step in GDGT synthesis requires the cell to supply not only e^-, but also additional chemical energy to re-reduce the co-factors.

Lipid biosynthesis is one of many components of cellular metabolism in ammonia-oxidizing Thaumarchaeota that require ATP- or proton motive force-dependent reverse electron flow. All of these pathways are in direct competition for both e^- and energy – the scarcity of which has been proposed as motivation for the evolution of the HP/HB pathway (59). The presence of cyclopentane rings in GDGTs may be viewed as an additional, analogous strategy to reduce demand for e^- and energy, as well as in the more traditional sense of producing a rigidified lipid

structure that aids in maintaining low proton permeability (37, 50). If there is an insufficient rate of $FADH_2$ regeneration under energy-limited conditions, DGGGP may utilize intramolecular e^--transfer, retaining the double-bond equivalent as a cycloalkyl ring (Fig. 5b).

This hypothesis offers a direct, mechanistic explanation for greater numbers of cycloalkyl rings at lower ammonia oxidation rates. If the production of more rings (and therefore higher TEX_{86} and RI values) is linked to the rate of $FADH_2$-regeneration, this effect should be more strongly expressed at lower oxidation rates. Our chemostat data, as well as previous batch culture studies from which oxidation rates may be inferred (Fig. 3; (34, 35) are consistent with this idea, as the number of rings (RI) scales directly with respiratory activity as expressed in the abundance of the electron carrier MK (Fig. 2b) and the ammonia oxidation rate.

Environmental implications. Our results suggest that the process of GDGT cyclization is at least partially decoupled from *direct* control by growth temperature, while simultaneously explaining how an *apparent* link to temperature may arise. Net primary production varies in response to density stratification and its effect on nutrient exchange through vertical mixing (66). This explains why warm environments with lower rates of both primary production and sub-photic zone nutrient regeneration, *i.e.*, lower ammonia oxidation rates (23, 67), have warm TEX_{86}-calibrated SSTs. Moreover, our results suggest that the TEX_{86} warming observed in oxygen minimum zones is caused by energy stress and corresponding decreased ammonia oxidation rates – *i.e.*, it is not directly caused by physiological response to low O_2. This explains why the subsurface TEX_{86} warming trend is observed in well-oxygenated water columns and not limited to oxygen minimum zones (28, 32, 35).

Further experiments with a broader range of thaumarchaeal ecotypes are necessary to understand the global relationship between TEX_{86} and ammonia oxidation rates. *N. maritimus* was isolated from a tropical fish tank in the Seattle aquarium (19) and displays a narrow growth range (~20-30°C) and a high temperature optimum (28°C), which is particularly applicable to the low latitude environment studied here. However the global TEX_{86} calibration encompasses temperate and polar eco- and phylotypes (68, 69) that may exhibit different magnitudes for the relationship between TEX_{86} and ammonia oxidation rate (Eq. 1), as evidenced by latitude-dependent and ocean basin-dependent TEX_{86} patterns (52). Nevertheless, it is encouraging that the inverse correlation between TEX_{86} and ammonia oxidation rate determined for a single taxon, *N. maritimus*, agrees with patterns of TEX_{86} values produced by natural assemblages in the marine water column. This suggests it is a universal mechanism among marine archaea.

Finally, our findings suggest that it may be challenging to accurately interpret the relationship between TEX_{86} ratios and SSTs in past ocean regimes in which circulation-driven nutrient regeneration rates or total global nutrient budgets may have had different patterns and thus different correlations to regional temperatures. The TEX_{86}-SST calibration likely is governed by the structure of the nutricline and its relationship to ocean thermal properties. This attribute of the TEX_{86} ratio may make it a promising tracer for understanding the ocean's nutrient dynamics and patterns of paleoproductivity.

Methods

Chemostat cultivation. *N. maritimus* SCM1 was maintained at 28°C and pH 7.6 in the dark in a 4.5-l chemostat containing Synthetic Crenarchaeota Medium (150 µM NH_4^+; Fig. S2; (19, 57), described in detail in the SI Appendix, Materials and Methods. Specific growth rate (d^{-1}) was controlled by dilution with fresh medium and three steady-state experiments were performed (slow stage, 0.23 d^{-1}, 71 h T_d; middle stage, 0.56 d^{-1}, 30 h T_d; fast stage, 0.75 d^{-1}, 22 h T_d; Fig S3).

Water column sampling. Depth profiles of (SPM) samples were retrieved from a latitudinal transect through the Atlantic Ocean during the DeepDOM cruise aboard R/V *Knorr* in 2013 (Fig. S5) using *in situ* pumps equipped with a sequence of filters (53 µm, 0.7 µm, 0.3 µm).

Lipid Extraction and Analysis. Lipids were extracted from biomass harvested from chemostat effluent by cross-flow filtration or centrifugation. Intact polar lipids and quinones from biomass and SPM were analyzed using reversed phase high performance liquid chromatography–mass spectrometry (HPLC–MS; (70). Core lipids extracted from hydrolyzed biomass were analyzed using normal phase HPLC–MS (71). For details, see SI Appendix, Materials and Methods.

Acknowledgments.

The authors thank Joe Jennings (Oregon State University) for nitrite concentrations. Funding for the cruise was provided by the National Science Foundation (OCE-1154320 to E. Kujawinski and K. Longnecker, WHOI). This research was supported by the Deutsche Forschungsgemeinschaft through the Gottfried Wilhelm Leibniz Program (award to KUH; Hi 616-14-1, funds for FJE, MK, construction of chemostat, acquisition of ABSciEX QTRAP4500 mass spectrometer) and instrument grant Inst 144/300-1 (qToF-MS). AP and SJH acknowledge funding from the National Science Foundation (OCE-1129343), the Gordon and Betty Moore Foundation, an EAOG travel fellowship, and the NASA Astrobiology Institute. **Author contributions** S.J.H., F.J.E., M.K., K.-U.H., and A.P. designed research; S.J.H., F.J.E., J.S.L., C.B., A.E.S., S.D.W. performed research; S.J.H., F.J.E. and A.P. analyzed data; and S.J.H., F.J.E., M.K., K.-U.H., A.P. wrote the paper with input from all co-authors.

1. Schouten S, Hopmans EC, Schefuß E, Sinninghe Damsté JS (2002) Distributional variations in marine crenarchaeotal membrane lipids: a new tool for reconstructing ancient sea water temperatures? *Earth Planet Sci Lett* 204(1-2):265–274.
2. Zachos JC, et al. (2006) Extreme warming of mid-latitude coastal ocean during the Paleocene-Eocene Thermal Maximum: Inferences from TEX_{86} and isotope data. *Geology* 34(9):737.
3. Schouten S, et al. (2003) Extremely high sea-surface temperatures at low latitudes during the middle Cretaceous as revealed by archaeal membrane lipids. *Geology* 31(12):1069.
4. Shevenell AE, Ingalls AE, Domack EW, Kelly C (2011) Holocene Southern Ocean surface temperature variability west of the Antarctic Peninsula. *Nature* 470(7333):250–254.
5. Huguet C, Kim J-H, Sinninghe Damsté JS, Schouten S (2006) Reconstruction of sea surface temperature variations in the Arabian Sea over the last 23 kyr using organic proxies (TEX_{86} and $U^{K'}_{37}$). *Paleoceanography* 21(3):DOI: 10.1029/2005PA001215.
6. Tierney JE, et al. (2010) Late-twentieth-century warming in Lake Tanganyika unprecedented since AD 500. *Nat Geosci* 3(6):422–425.
7. Brochier-Armanet C, Boussau B, Gribaldo S, Forterre P (2008) Mesophilic Crenarchaeota: proposal for a third archaeal phylum, the Thaumarchaeota. *Nat Rev Microbiol* 6(3):245–52.
8. Spang A, et al. (2010) Distinct gene set in two different lineages of ammonia-oxidizing archaea supports the phylum Thaumarchaeota. *Trends Microbiol* 18(8):331–40.
9. Pitcher A, et al. (2011) Core and intact polar glycerol dibiphytanyl glycerol tetraether lipids of ammonia-oxidizing archaea enriched from marine and estuarine sediments. *Appl Environ Microbiol* 77(10):3468–77.
10. Schouten S, et al. (2008) Intact membrane lipids of "*Candidatus* Nitrosopumilus maritimus," a cultivated representative of the cosmopolitan mesophilic group I Crenarchaeota. *Appl Environ Microbiol* 74(8):2433–40.
11. Schouten S, Hopmans EC, Pancost RD, Damste JS (2000) Widespread occurrence of structurally diverse tetraether membrane lipids: evidence for the ubiquitous presence of low-temperature relatives of hyperthermophiles. *Proc Natl Acad Sci U S A* 97(26):14421–6.
12. Damste JSS (2002) Crenarchaeol: the characteristic core glycerol dibiphytanyl glycerol tetraether membrane lipid of cosmopolitan pelagic crenarchaeota. *J Lipid Res* 43(10):1641–1651.
13. Hoefs M, et al. (1997) Ether lipids of planktonic archaea in the marine water column. *Appl Environ Microbiol* 63(8):3090–3095.
14. Lincoln SA, et al. (2014) Planktonic Euryarchaeota are a significant source of archaeal tetraether lipids in the ocean. *Proc Natl Acad Sci U S A* 111(27):1409439111–.
15. Biddle JF, et al. (2006) Heterotrophic Archaea dominate sedimentary subsurface ecosystems off Peru. *Proc Natl Acad Sci U S A* 103(10):3846–51.
16. Lipp JS, Hinrichs K-U (2009) Structural diversity and fate of intact polar lipids in marine sediments. *Geochim Cosmochim Acta* 73(22):6816–6833.
17. Kim J-H, et al. (2010) New indices and calibrations derived from the distribution of crenarchaeal isoprenoid tetraether lipids: Implications for past sea surface temperature reconstructions. *Geochim Cosmochim Acta* 74(16):4639–4654.
18. Tierney JE, Tingley MP (2014) A Bayesian, spatially-varying calibration model for the TEX_{86} proxy. *Geochim Cosmochim Acta* 127:83–106.
19. Könneke M, et al. (2005) Isolation of an autotrophic ammonia-oxidizing marine archaeon. *Nature* 437(7058):543–6.
20. Church MJ, Wai B, Karl DM, DeLong EF (2010) Abundances of crenarchaeal *amoA* genes and transcripts in the Pacific Ocean. *Environ Microbiol* 12(3):679–88.
21. Francis CA, Roberts KJ, Beman JM, Santoro AE, Oakley BB (2005) Ubiquity and diversity of ammonia-oxidizing archaea in water columns and sediments of the ocean. *Proc Natl Acad Sci U S A* 102(41):14683–8.
22. Karner MB, DeLong EF, Karl DM (2001) Archaeal dominance in the mesopelagic zone of the Pacific Ocean. *Nature* 409(6819):507–10.
23. Santoro AE, Casciotti KL, Francis CA (2010) Activity, abundance and diversity of nitrifying

archaea and bacteria in the central California Current. *Environ Microbiol* 12(7):1989–2006.
24. Taylor KWR, Huber M, Hollis CJ, Hernandez-Sanchez MT, Pancost RD (2013) Re-evaluating modern and Palaeogene GDGT distributions: Implications for SST reconstructions. *Glob Planet Change* 108:158–174.
25. Pearson A, McNichol AP, Benitez-Nelson BC, Hayes JM, Eglinton TI (2001) Origins of lipid biomarkers in Santa Monica Basin surface sediment: a case study using compound-specific Δ14C analysis. *Geochim Cosmochim Acta* 65(18):3123–3137.
26. Ingalls AE, et al. (2006) Quantifying archaeal community autotrophy in the mesopelagic ocean using natural radiocarbon. *Proc Natl Acad Sci U S A* 103(17):6442–7.
27. Shah SR, Mollenhauer G, Ohkouchi N, Eglinton TI, Pearson A (2008) Origins of archaeal tetraether lipids in sediments: Insights from radiocarbon analysis. *Geochim Cosmochim Acta* 72(18):4577–4594.
28. Basse A, et al. (2014) Distribution of intact and core tetraether lipids in water column profiles of suspended particulate matter off Cape Blanc, NW Africa. *Org Geochem* 72:1–13.
29. Wuchter C, Schouten S, Wakeham SG, Sinninghe Damsté JS (2005) Temporal and spatial variation in tetraether membrane lipids of marine Crenarchaeota in particulate organic matter: Implications for TEX_{86} paleothermometry. *Paleoceanography* 20(3):DOI: 10.1029/2004PA001110.
30. Turich C, et al. (2007) Lipids of marine Archaea: Patterns and provenance in the water-column and sediments. *Geochim Cosmochim Acta* 71(13):3272–3291.
31. Schouten S, et al. (2012) Intact polar and core glycerol dibiphytanyl glycerol tetraether lipids in the Arabian Sea oxygen minimum zone: I. Selective preservation and degradation in the water column and consequences for the TEX_{86}. *Geochim Cosmochim Acta* 98:228–243.
32. Hernández-Sánchez MT, et al. (2014) Variations in GDGT distributions through the water column in the South East Atlantic Ocean. *Geochim Cosmochim Acta* 132:337–348.
33. Xie S, Liu X-L, Schubotz F, Wakeham SG, Hinrichs K-U (2014) Distribution of glycerol ether lipids in the oxygen minimum zone of the Eastern Tropical North Pacific Ocean. *Org Geochem* 71:60–71.
34. Elling FJ, et al. (2014) Effects of growth phase on the membrane lipid composition of the thaumarchaeon Nitrosopumilus maritimus and their implications for archaeal lipid distributions in the marine environment. *Geochim Cosmochim Acta* 141:579–597.
35. Qin W, et al. (2015) Confounding effects of oxygen and temperature on the TEX_{86} signature of marine Thaumarchaeota. *Proc Natl Acad Sci U S A* 112(35):10979–10984.
36. Valentine DL (2007) Adaptations to energy stress dictate the ecology and evolution of the Archaea. *Nat Rev Microbiol* 5(4):316–23.
37. Elferink MGL, de Wit JG, Driessen AJM, Konings WN (1994) Stability and proton-permeability of liposomes composed of archaeal tetraether lipids. *Biochim Biophys Acta - Biomembr* 1193(2):247–254.
38. Van de Vossenberg JLCM, Driessen AJM, Konings WN (1998) The essence of being extremophilic: the role of the unique archaeal membrane lipids. *Extremophiles* 2(3):163–170.
39. Popp BN, et al. (1998) Effect of Phytoplankton Cell Geometry on Carbon Isotopic Fractionation. *Geochim Cosmochim Acta* 62(1):69–77.
40. Laws EA, Popp BN, Bidigare RR, Kennicutt MC, Macko SA (1995) Dependence of phytoplankton carbon isotopic composition on growth rate and $[CO_2]_{aq}$: Theoretical considerations and experimental results. *Geochim Cosmochim Acta* 59(6):1131–1138.
41. Riegman R, Stolte W, Noordeloos AAM, Slezak D (2000) Nutrient uptake and alkaline phosphatase (ec 3:1:3:1) activity of *emiliania huxleyi* (prymnesiophyceae) during growth under n and p limitation in continuous cultures. *J Phycol* 36(1):87–96.
42. Elling FJ, Könneke M, Mußmann M, Greve A, Hinrichs K-U (2015) Influence of temperature, pH, and salinity on membrane lipid composition and TEX_{86} of marine planktonic thaumarchaeal isolates. *Geochim Cosmochim Acta*:doi:10.1016/j.gca.2015.09.004.
43. Wuchter C, Schouten S, Coolen MJL, Sinninghe Damsté JS (2004) Temperature-dependent variation in the distribution of tetraether membrane lipids of marine Crenarchaeota: Implications for TEX_{86} paleothermometry. *Paleoceanography* 19(4):doi:10.1029/2004PA001041.
44. Collins MD (1994) Isoprenoid Quinones. *Chemical Methods in Prokaryotic Systematics*, eds Goodfellow M, O'Donnell AG (John Wiles, Chichester, UK), pp 265–309.
45. Smith JM, Casciotti KL, Chavez FP, Francis CA (2014) Differential contributions of archaeal ammonia oxidizer ecotypes to nitrification in coastal surface waters. *ISME J* 8(8):1704–14.
46. Santoro AE, Casciotti KL (2011) Enrichment and characterization of ammonia-oxidizing archaea from the open ocean: phylogeny, physiology and stable isotope fractionation. *ISME J* 5(11):1796–808.
47. Santoro AE, et al. (2015) Genomic and proteomic characterization of " Candidatus Nitrosopelagicus brevis": An ammonia-oxidizing archaeon from the open ocean. *Proc Natl Acad Sci U S A* 112(4):1173–1178.
48. Wuchter C, et al. (2006) Archaeal nitrification in the ocean. *Proc Natl Acad Sci U S A* 103(33):12317–22.
49. Uda I, Sugai A, Itoh YH, Itoh T (2001) Variation in molecular species of polar lipids from Thermoplasma acidophilum depends on growth temperature. *Lipids* 36(1):103–105.
50. Chong PL-G (2010) Archaebacterial bipolar tetraether lipids: Physico-chemical and membrane properties. *Chem Phys Lipids* 163(3):253–65.
51. Koga Y (2012) Thermal adaptation of the archaeal and bacterial lipid membranes. *Archaea* 2012:789652.
52. Pearson A, Ingalls AE (2013) Assessing the Use of Archaeal Lipids as Marine Environmental Proxies. *Annu Rev Earth Planet Sci* 41(1):359–384.
53. Schouten S, Hopmans EC, Sinninghe Damsté JS (2013) The organic geochemistry of glycerol dialkyl glycerol tetraether lipids: A review. *Org Geochem* 54:19–61.
54. Oger PM, Cario A (2013) Adaptation of the membrane in Archaea. *Biophys Chem* 183:42–56.
55. Meador TB, et al. (2014) Thermococcus kodakarensis modulates its polar membrane lipids and elemental composition according to growth stage and phosphate availability. *Front Microbiol* 5:10.
56. Yoshinaga MY, et al. (2015) Methanothermobacter thermautotrophicus modulates its membrane lipids in response to hydrogen and nutrient availability. *Front Microbiol* 6:5.
57. Martens-Habbena W, Berube PM, Urakawa H, de la Torre JR, Stahl DA (2009) Ammonia oxidation kinetics determine niche separation of nitrifying Archaea and Bacteria. *Nature* 461(7266):976–9.
58. Horak REA, et al. (2013) Ammonia oxidation kinetics and temperature sensitivity of a natural marine community dominated by Archaea. *ISME J* 7(10):2023–33.
59. Könneke M, et al. (2014) Ammonia-oxidizing archaea use the most energy-efficient aerobic pathway for CO2 fixation. *Proc Natl Acad Sci U S A* 111(22):8239–44.
60. Qin W, et al. (2014) Marine ammonia-oxidizing archaeal isolates display obligate mixotrophy and wide ecotypic variation. *Proc Natl Acad Sci U S A* 111(34):12504–9.
61. Ouverney CC, Fuhrman JA (2000) Marine Planktonic Archaea Take Up Amino Acids. *Appl Environ Microbiol* 66(11):4829–4833.
62. Tourna M, et al. (2011) Nitrososphaera viennensis, an ammonia oxidizing archaeon from soil. *Proc Natl Acad Sci U S A* 108(20):8420–5.
63. Nishimura Y, Eguchi T (2006) Biosynthesis of archaeal membrane lipids: digeranylgeranylglycerophospholipid reductase of the thermoacidophilic archaeon Thermoplasma acidophilum. *J Biochem* 139(6):1073–81.
64. Walker CB, et al. (2010) Nitrosopumilus maritimus genome reveals unique mechanisms for nitrification and autotrophy in globally distributed marine crenarchaea. *Proc Natl Acad Sci U S A* 107(19):8818–23.
65. Sasaki D, et al. (2011) Structure and mutation analysis of archaeal geranylgeranyl reductase. *J Mol Biol* 409(4):543–57.
66. Behrenfeld MJ, et al. (2006) Climate-driven trends in contemporary ocean productivity. *Nature* 444(7120):752–5.
67. Newell SE, Babbin AR, Jayakumar A, Ward BB (2011) Ammonia oxidation rates and nitrification in the Arabian Sea. *Global Biogeochem Cycles* 25(4):DOI: 10.1029/2010GB003940.
68. Pester M, Schleper C, Wagner M (2011) The Thaumarchaeota: an emerging view of their phylogeny and ecophysiology. *Curr Opin Microbiol* 14(3):300–6.
69. Luo H, et al. (2014) Single-cell genomics shedding light on marine Thaumarchaeota diversification. *ISME J* 8(3):732–6.
70. Zhu C, et al. (2013) Comprehensive glycerol ether lipid fingerprints through a novel reversed phase liquid chromatography–mass spectrometry protocol. *Org Geochem* 65:53–62.
71. Becker KW, Lipp JS, Zhu C, Liu X-L, Hinrichs K-U (2013) An improved method for the analysis of archaeal and bacterial ether core lipids. *Org Geochem* 61:34–44.
72. Strickland JDH, Parsons TR (1972) *A parctical Handbook of Seawater Analysis* doi:10.100-2/iroh.19700550118.
73. Lunau M, Lemke A, Walther K, Martens-Habbena W, Simon M (2005) An improved method for counting bacteria from sediments and turbid environments by epifluorescence microscopy. *Environ Microbiol* 7(7):961–8.
74. Herbert D, Elsworth R, Telling RC (1956) The Continuous Culture of Bacteria; a Theoretical and Experimental Study. *J Gen Microbiol* 14(3):601–622.
75. Sturt HF, Summons RE, Smith K, Elvert M, Hinrichs K-U (2004) Intact polar membrane lipids in prokaryotes and sediments deciphered by high-performance liquid chromatography/electrospray ionization multistage mass spectrometry--new biomarkers for biogeochemistry and microbial ecology. *Rapid Commun Mass Spectrom* 18(6):617–28.
76. Zhang CL, Pearson A, Li Y-L, Mills G, Wiegel J (2006) Thermophilic temperature optimum for crenarchaeol synthesis and its implication for archaeal evolution. *Appl Environ Microbiol* 72(6):4419–22.
77. Kujawinski E., et al. (2013) DeepDOM cruise report, BCO-DMO public data: http://www.bco-dmo.org/project/2204.

Please review all the figures in this paginated PDF and check if the figure size is appropriate to allow reading of the text in the figure.

If readability needs to be improved then resize the figure again in 'Figure sizing' interface of Article Sizing Tool.